Geophys. J. Int. (2004) **157,** 117–127 doi: 10.1111/j.1365-246X.2004.02225.x

A method for the separation of paramagnetic, ferrimagnetic and haematite magnetic subfabrics using high-field torque magnetometry

Fátima Martín-Hernández[1] and Ann M. Hirt[2]

[1]*Paleomagnetic Laboratory 'Fort Hoofddijk', Faculty of Geosciences, Utrecht University, Budapestlaan* 17, *Utrecht* 3584 CD, *the Netherlands. E-mail: fatima@geo.uu.nl*

[2]*Institute of Geophysics, ETH-Hönggerberg, Zürich* CH-8093, *Switzerland. E-mail: hirt@mag.ig.erdw.ethz.ch*

Accepted 2003 December 16. Received 2003 November 10; in original form 2003 June 9

SUMMARY

In this study, the contribution of the paramagnetic, ferrimagnetic and haematite components to the magnetic anisotropy is separated by means of high-field torque magnetometry. Torque measurements at different fields, which are high enough to saturate the ferrimagnetic minerals, however, still low enough that the torque resulting from the haematite is linear with field, allow for the separation of the three magnetic anisotropy components. The method has been applied to haematite single crystals in which no paramagnetic or ferrimagnetic components have been found contribute to the torque signal. The mean direction of the poles to the crystallographic basal plane in the haematite single crystals is subparallel to the minimum-susceptibility direction measured in low-field. The separation analysis has also been applied to highly deformed red beds from the Lower Glarus nappe complex (Switzerland). No ferrimagnetic phases are present in the rocks and, therefore, they cannot contribute to the anisotropy of magnetic susceptibility. The magnetic fabric arises from a paramagnetic subfabric carried by the phyllosilicate minerals and haematite, in which the basal planes of both phases are in the cleavage plane. The measured magnetic lineation seen in low-field anisotropy of magnetic susceptibility appears to be an apparent lineation that arises from a weak girdling of haematite and the paramagnetic minerals conforming the rock.

Key words: ferromagnetic, haematite, high-field torque magnetometer, paramagnetism, rock magnetism.

1 INTRODUCTION

Anisotropy of magnetic susceptibility (AMS) is determined from the directional variability of the magnetization (M_i) in an applied field (B_j). It can be described mathematically as a symmetric second-rank tensor (k_{ij}) and can be represented physically by an ellipsoid with three principal axes. For the anisotropy of the magnetic susceptibility the eigenvalues corresponding to principal axes are given by $k_1 \geq k_2 \geq k_3$. Many studies have shown a qualitative correlation between anisotropy of magnetic susceptibility and mineral and tectonic fabrics (e.g. Hrouda 1982; Rochette *et al.* 1992; Tarling & Hrouda 1993; Borradaile & Henry 1997).

Standard low-field AMS measurements apply weak fields (*ca* 300 A m^{-1}) where the magnetization is reversible. With this technique all the minerals present in the sample contribute to the AMS, although it is often dominated by the ferromagnetic phases (e.g. Tarling & Hrouda 1993). However, it has been revealed in some cases that the magnetic anisotropy is carried by the paramagnetic minerals forming the rock (Hounslow 1985; Borradaile *et al.* 1985/86; Hirt *et al.* 2000; Parés & van der Pluijm 2002b). Low-field measurements of the AMS present an additional problem in haematite-bearing rocks. In haematite single crystals the minimum susceptibility calculated by the KLY-2 susceptibility bridge has negative values because the susceptibility magnitude ellipsoid is rotational oblate (Hrouda 2002a). In this case, the measurements do not fit into a triaxial ellipsoid because it degenerates into a plane.

Many methods have been proposed to separate the magnetic anisotropy subfabrics in samples composed of paramagnetic and ferromagnetic minerals. Some methods are based on the temperature dependence of the paramagnetic phases (Richter & van der Pluijm 1994; Parés & van der Pluijm 2002a,b). These methods only separate the paramagnetic phases, however, they do not distinguish between ferrimagnetic phases and haematite. Another approach is the use of anisotropy of remanence magnetization (ARM) for the determination of anisotropy of the ferromagnetic minerals (McCabe *et al.* 1985; Jackson 1991). A mathematical evaluation of low-field AMS and ARM permits the separation of paramagnetic and ferromagnetic subfabrics (Hrouda 2002b). High-field methods based on hysteresis measurements have also been proposed to separate the paramagnetic contribution to the magnetic fabric (Borradaile & Werner 1994; Kelso *et al.* 2002). These methods, unfortunately, are not applicable to haematite-bearing rocks because saturation of this

high-coercivity mineral is not reached in most commercial instruments. Rochette & Fillion (1988) used a cryogenic magnetometer to determined the susceptibility of the different magnetic fractions by exploiting the field dependence of the magnetization curves up to 4 T at room temperature. An alternative high-field method is a high-field torque magnetometer, which has been proved to be effective in separating the magnetic subfabrics resulting from paramagnetic and ferrimagnetic phases (Hrouda & Jelinek 1990; Martín-Hernández & Hirt 2001, 2003). Friedrich *et al.*(1995) proposed a method based on high-field torque measurements to calculate the paramagnetic and ferrimagnetic fabrics when the ferromagnetic fabric is pyrrhotite and/or haematite with the auxiliary help of the energy density parameter.

Magnetic torque measurements on haematite single crystals have been carried out in early studies to calculate magnetization intensity as a function of applied field (Townsend 1920; Tasaki & Iida 1963; Flanders & Remeika 1965). The torque of haematite crystals has also been used to investigate the variation of the magnetization with temperature (Flanders & Remeika 1965) and the anisotropy of haematite plates within the basal plane (Flanders & Schuele 1964). A mathematical model that explains the observed torque curves was proposed by Porath & Chamalaun (1966). The applicability of the high-field torque measurements for determining the AMS in haematite was initially rejected because the torque curve is asymmetric with the orientation angle. However, the same model was used by Jelinek (1985) to describe the energy density tensor of haematite and by Rochette & Fillion (1988) for the high-field magnetization of haematite-bearing rocks.

In this paper, a new mathematical method is presented that separates the magnetic anisotropy components in samples where haematite also contributes to the AMS. It is a generalization of the model presented by Porath & Chamalaun (1966), who assumed that the haematite plate is initially oriented at zero degrees with respect to the haematite plate and the rotational plane intercept. It compliments the method presented by Martín-Hernández & Hirt (2001), which is restricted to samples with paramagnetic and saturated ferrimagnetic contributions to the AMS.

The new method is based on the measurement of torque in several fields, which can range from 0.045 to 1.8 T, using a high-field torque magnetometer. Paramagnetic and/or diamagnetic, haematite and low-coercivity ferrimagnetic minerals show different dependencies of the torque curve with the applied field. The different behaviour of the torque curves with respect to the applied field is used to separate the contribution of the three groups of minerals to the torque signal. Each contribution is further fitted by the best theoretical curve for the evaluation of the magnetic ellipsoids of the different subfabrics.

2 SEPARATION OF MAGNETIC ANISOTROPY COMPONENTS

The different dependencies between the applied field and the measured torque for the paramagnetic minerals, haematite and ferrimagnetic minerals above their saturation is shown in Fig. 1. It illustrates an example of a torque signal and its corresponding amplitude for the three types of minerals. The torque resulting from the paramagnetic and/or diamagnetic fraction is linearly dependent on the square of applied field (Banerjee & Stacey 1967; Collinson *et al.* 1967; Hrouda & Jelinek 1990; Martín-Hernández & Hirt 2001). The diamagnetic contribution will be considered neglectible, however, in samples where it contributes to the magnetic anisotropy it will be included in the paramagnetic term (Martín-Hernández & Hirt 2001). Fig. 1(a) shows torque of a biotite single crystal measured at different fields in a non-basal plane. Fig. 1(b) illustrates the computed amplitude of the torque signal as a function of the applied field for an antiferromagnetic mineral, e.g. haematite or pyrrhotite. The torque of haematite single crystals has been reported to be linearly field-dependent at room temperature (Townsend 1920; Flanders & Remeika 1965; Porath & Chamalaun 1966; Hrouda *et al.* 1985). It is characterized by asymmetry and a sudden drop in the torque signal that corresponds to the orientation in which the magnetization changes the orientation 180° within the basal plane (Fig. 1c). The amplitude of the torque signal is proportional to the applied field (Fig. 1d). For ferrimagnetic minerals above their saturation, the magnetic torque is constant with field (Banerjee & Stacey 1967; Collinson *et al.* 1967; Hrouda & Jelinek 1990; Martín-Hernández & Hirt 2001) (Fig. 1e). The corresponding amplitude of the torque signal is, therefore, constant with applied field because the titanomagnetite has reached saturation (Fig. 1f).

For natural samples containing a mixture of anisotropic magnetic minerals, the resulting torque can be divided into the sum of the three terms if the ferrimagnetic fraction is saturated. The total torque signal of the sample, rotated in the $x_1 - x_2$ plane of an orthogonal coordinate system ($x_1 - x_2 - x_3$), is exerted in the x_3 direction and it is described by the addition of the following terms:

$$t_3^{\text{total}} = t_3^{\text{para}}(B^2) + t_3^{\text{hem}}(B) + t_3^{\text{ferri}} \quad (1)$$

For every angle in which the sample is measured at the field B the decomposition of the torque signal from eq. (1) is valid. By fitting the torque with a second-order polynomial, each carrier of the magnetic anisotropy is identified by one coefficient:

$$t_3^{\text{total}}(\theta) = a_3(\theta)B^2 + b_3(\theta)B + c_3(\theta) \quad (2)$$

Comparing eqs (1) and (2), $c_3\ (\theta)$ is the coefficient of the torque the ferrimagnetic phases above their saturation, $b_3\ (\theta)$ is the coefficient of the torque resulting from haematite and $a_3\ (\theta)$ the coefficient of the torque resulting from the paramagnetic minerals. If the calculation is repeated for all the angles of measurements between 0° and 360° in three perpendicular planes, the corresponding torque component for each of the three magnetic mineral types can be calculated. The significance of the coefficients are evaluated with their 95 per cent confidence limits assuming the original data to be independent normal with equal variance (Cheeney 1983). The error estimation of the fit is obtained from the covariance matrix, which gives a standard deviation for each coefficient. This is used to calculate the 95 per cent confidence limit. The error band or fiducial limits on every curve provides a tool for the discrimination for the statistical significance of the computed fitting. Curves in which more than 50 per cent of the points are not statistically different from zero have been considered to be insignificant for the evaluation of the associated components.

The paramagnetic $[a_i(\theta)]$, haematite $[b_i(\theta)]$ and ferrimagnetic $[c_i(\theta)]$ coefficients are calculated for a discrete number of orientation angles between 0° and 360° in three perpendicular planes ($i = 1, 2, 3$). A total of nine curves are calculated for each sample after this process. The computed coefficients can be shifted with respect to the horizontal axes as a result of the strong rotational hysteresis of haematite (Townsend 1920; Flanders & Schuele 1964). Above approximately 0.5 T, the rotational hysteresis term decreases with the applied field to a constant term with a dependency of $1/B$,$1/B^2$ or a combination of both (Owens 1981). The rotational hysteresis is, therefore, coupled with the paramagnetic, haematite and/or ferrimagnetic coefficient depending on many factors, such as

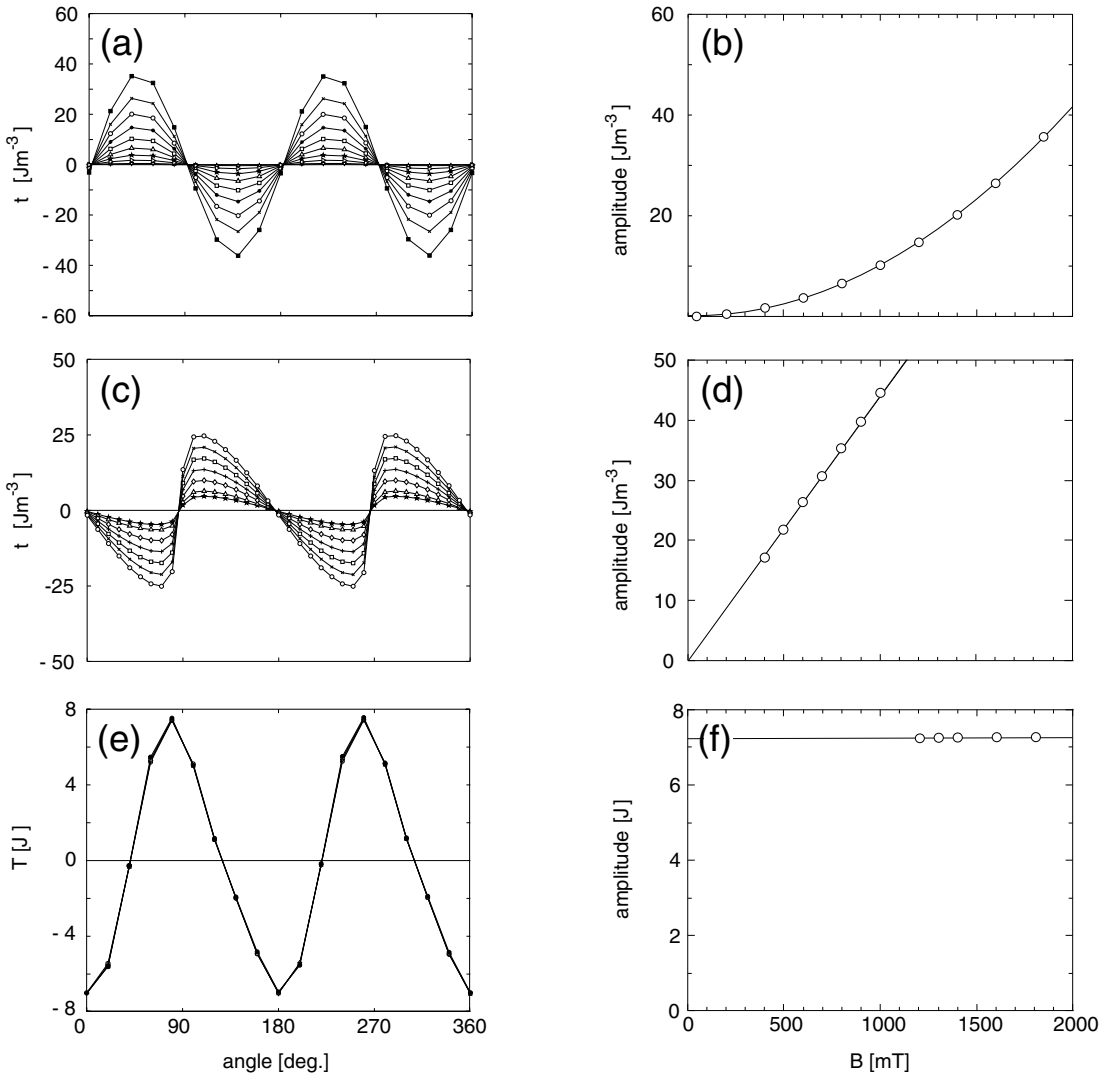

Figure 1. Torque as a function of angle (left) and corresponding amplitude of the torque signal as a function of applied field (right) for three different types of magnetic minerals. Biotite single crystal in a plane perpendicular to the crystal cleavage (a, b), haematite-plate single crystal in a plane perpendicular to the crystal cleavage (c, d) and titanomagnetite (e, f). Note that (e) and (f) show the total torque without being normalized by volume.

grain size, mineral alteration and orientation of the haematite platelets (Brooks & O'Reilly 1970; Day *et al.* 1970; Owens 1981; Schmidbauer & Keller 1996).

The following is a short mathematical description for deriving the paramagnetic, ferrimagnetic and haematite components to the torque signal. A more complete derivation of the paramagnetic and ferrimagnetic equations is given by Jelinek (1985) and Martín-Hernández & Hirt (2001), and the general haematite equation in Porath & Chamalaun (1966) and Owens (1981).

2.1 Orientation of the paramagnetic component

The torque curve of a pure paramagnetic mineral that is rotated 360° in the $x_1 - x_2$ plane is a vector $[t_3^{\text{para}}(\theta)]$ in the x_3 direction. It is a function of the orientation angle and the square of the applied field (Banerjee & Stacey 1967; Collinson *et al.* 1967; Martín-Hernández & Hirt 2001):

$$t_3^{\text{para}} = \frac{1}{2\mu_o} B^2 [(k_{22} - k_{11}) \sin 2\theta + 2k_{12} \cos 2\theta] \tag{3}$$

where B is the strength of the applied field in T, k_{ij} are the terms of the paramagnetic susceptibility tensor in the sample coordinate system in SI units, θ is the angle of orientation of the applied field with respect to the sample coordinate system and μ_o is the magnetic permeability of vacuum. Measuring in three perpendicular planes, the coefficients of sine (A_i) and cosine (B_i) of 2θ are related with the six terms of the paramagnetic susceptibility tensor (Jelinek 1985; Martín-Hernández & Hirt 2001). It is not possible to compute the full paramagnetic susceptibility tensor because the equation system is described by differences of the matrix terms. Therefore, the solution requires the boundary condition $A_1 + A_2 + A_3 = 0$. The terms of the deviatoric paramagnetic susceptibility tensor can be computed from the following solution of the equation system where the superindex dev indicates that we solve only the deviatoric part.

$$\begin{aligned} k_{11}^{\text{dev}} &= \frac{2}{3}\mu_o(A_2 - A_3) \quad k_{12}^{\text{dev}} = \mu_o B_3 \\ k_{22}^{\text{dev}} &= \frac{2}{3}\mu_o(A_3 - A_1) \quad k_{23}^{\text{dev}} = \mu_o B_1 \\ k_{33}^{\text{dev}} &= \frac{2}{3}\mu_o(A_1 - A_2) \quad k_{13}^{\text{dev}} = \mu_o B_2 \end{aligned} \tag{4}$$

2.2 Orientation of the ferrimagnetic component

The torque curve of a ferrimagnetic mineral above its saturation that is rotated 360° in the $x_1 - x_2$ plane is a function of the orientation angle, however, it is independent of the applied field (Banerjee & Stacey 1967; Collinson *et al.* 1967; Martín-Hernández & Hirt 2001). The torque is expressed as:

$$t_3^{\text{ferri}} = \frac{1}{2}\mu_o M_S^2[(N_{22} - N_{11})\sin 2\theta + 2N_{12}\cos 2\theta] \tag{5}$$

where M_S is the saturation magnetization of the ferrimagnetic mineral and N_{ij} are the terms of the demagnetization factor tensor in the sample coordinate system.

The individual terms of the ferrimagnetic demagnetization factor tensor are computed, following the description outlined in the previous section, to solve the equation system. Each term of the ferrimagnetic demagnetization factor tensor is a function of the sine (C_i) and cosine (D_i) terms derived from Fourier analysis of the ferrimagnetic curves [c_i (θ)]. The superindex indicates that it is the deviatoric part.

$$\begin{aligned}
\mu_o^2 M_S^2 N_{11}^{\text{dev}} &= \frac{2}{3}(C_2 - C_3) \quad \mu_o^2 M_S^2 N_{12}^{\text{dev}} = D_3 \\
\mu_o^2 M_S^2 N_{22}^{\text{dev}} &= \frac{2}{3}(C_3 - C_1) \quad \mu_o^2 M_S^2 N_{23}^{\text{dev}} = D_1 \\
\mu_o^2 M_S^2 N_{33}^{\text{dev}} &= \frac{2}{3}(C_1 - C_2) \quad \mu_o^2 M_S^2 N_{13}^{\text{dev}} = D_2
\end{aligned} \tag{6}$$

2.3 Haematite component

The magnetization of haematite is given by the addition of two terms:

$$m = m_o + \chi B \tag{7}$$

where m is the magnetization vector, m_o is the parasitic ferromagnetic magnetization, χ is the magnetic susceptibility and B is the strength of the applied field. In a first approximation, it is possible to assume that the magnetization is a result of the ferromagnetic magnetization and that the ferromagnetic moment of haematite is confined to an isotropic basal plane. The validity of the simplification will be discussed below. The torque experienced by the sample can be described by the following formula:

$$\mathbf{t} = \mathbf{m}_{\text{H}} \times \mathbf{B} \tag{8}$$

where $\mathbf{t}$ is the magnetic torque (in J m^{-3}), $\mathbf{m}_{\text{H}}$ is the projection the ferromagnetic moment in the plane of rotation (in A m^{-1}) and $\mathbf{B}$ is the applied field (in T). The torque experienced by a haematite plate will depend on: (i) the orientation of the haematite basal plane with respect to the plane of rotation, (ii) the ferromagnetic moment and (iii) the orientation of the sample (Porath & Chamalaun 1966). Eq. (9) is a generalization of the theoretical curve proposed by Porath & Chamalaun (1966) and applies to any initial orientation of the intersection between the haematite basal plane and sample coordinate axis (θ_o).

$$t^{\text{hem}}(\theta) = \text{sign}[\cos(\theta - \theta_o)]\frac{m_o B \sin(\theta - \theta_o)\sin^2\varphi}{\sqrt{1 + \tan^2(\theta - \theta_o)\cos^2\varphi}} \tag{9}$$

where θ is the angle of rotation with respect to the sample coordinate system, θ_o is the initial orientation of the intersection of the two planes, φ is the angle between the haematite basal plane and the plane of rotation of the applied field, m_o is ferromagnetic moment, B is the strength of the applied field and sign(x) is the sign function which is defined as sign(x) = 1 for $x > 0$ and sign(x) = -1 for $x < 0$. Fig. 2 shows schematically the angular relationship between the orientation of the haematite crystal, the applied field and the coordinate system.

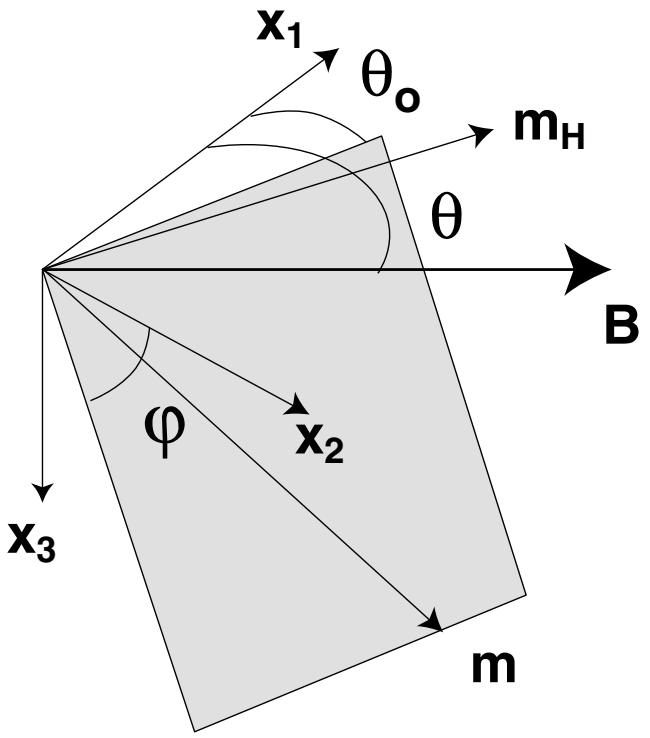

Figure 2. Schematic diagram of the angular relationship between the horizontal plane or plane of rotation, which contains the applied field and the orientation of a haematite plate (grey plane) (modified after Porath & Chamalaun 1966).

The curves derived are fitted with the theoretical model expressed in eq. (9) using a least-squares non-linear fitting with the ferromagnetic moment (m_o), orientation of the basal plane (φ) and initial orientation of the basal plane-rotational plane interception (θ_o) as unknown variables. This provides a mean orientation of the pole to basal planes of the haematite crystals for each measured plane.

3 EXPERIMENTAL METHOD

Low-field susceptibility was measured in all analysed samples with an AGICO (Brno, Czech Republic) KLY-2 susceptibility meter, in which the strength of the alternating field is 300 A m^{-1}. Fifteen independent measurement positions are used to define the susceptibility tensor (Jelinek 1978). The anisotropy of low-field magnetic susceptibility has been measured at 77 K in order to enhance the paramagnetic contribution to the low-field susceptibility (Lüneburg *et al.* 1999; Parés & van der Pluijm 2002a). The experimental procedure has been described by Lüneburg *et al.* (1999). The ratio between the bulk susceptibility at 77 K and at room temperature 293 K is used as an indicator of the paramagnetic content in the samples. For pure paramagnetic minerals following the Curie–Weiss law this ratio is approximately 3.8 (Lüneburg *et al.* 1999; Parés & van der Pluijm 2002a).

Samples were subsequently measured with a high-field torque magnetometer (Bergmüller *et al.* 1994). Each sample was measured during a full rotation of 360° in three perpendicular planes forming a dextral system. The samples were measured at intervals of 20° and one sample from each of the following examples at 10° intervals to test the convergence of the non-linear fitting of the haematite

fraction with a larger number of points. A minimum of six applied fields from 0.8 to 1.8 T were applied: these are strong enough to saturate the magnetization of the ferrimagnetic minerals magnetite, titanomagnetite and maghemite (e.g. Dunlop & Özdemir 1997).

Additional rock magnetic experiments have been done on the pilot samples from the red beds in order to identify the ferromagnetic minerals present in the samples. Acquisition of isothermal remanent magnetization (IRM) and thermal demagnetization of IRM cross components were measured to identify the ferromagnetic minerals present in the samples, following the method described by Lowrie (1990).

The shape and degree of anisotropy of the paramagnetic susceptibility ellipsoid cannot be represented on a standard Jelinek plot because it is only possible to compute deviatoric values of the susceptibility tensor (Hrouda & Jelinek 1990). Instead, an alternative parameter (U) can be calculated for the shape of the ellipsoid (Jelinek 1981; Hrouda 2002a).

$$U = \frac{2k_{22} - k_{11} - k_{33}}{k_{11} - k_{33}} \tag{10}$$

where k_{ij} are the terms of one susceptibility tensor. Values of $U > 0$, $U < 0$ and $U = 0$ correspond to oblate, prolate and neutral ellipsoids, respectively. The evaluation of the degree of anisotropy has been done using differences between k_1 and k_3 axes.

4 APPLICATIONS

4.1 Haematite single crystals

Two macroscopic, haematite single crystals from the Swiss Alps have been measured with both the low-field KLY-2 susceptibility bridge and the high-field torque magnetometer. Each of the

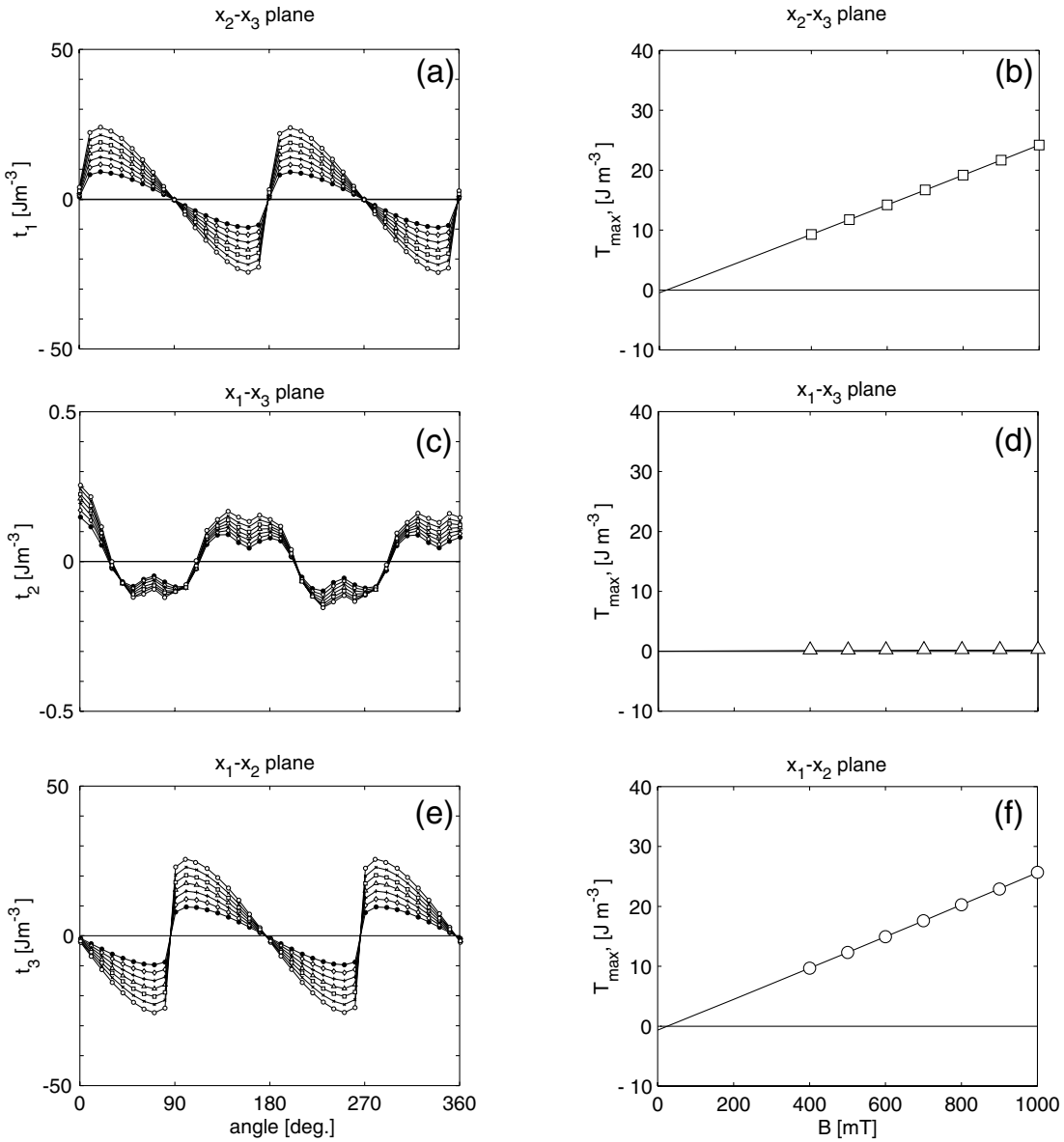

Figure 3. Torque curves (left) and corresponding amplitude of the torque signal (right) for a haematite single crystal measured. Plane $x_2 - x_3$ is perpendicular to the haematite basal plane (a, b), plane $x_1 - x_3$ is parallel to the haematite basal plane (c, d) and plane $x_1 - x_2$ is perpendicular to the haematite basal plane (e, f) in this and Fig. 4.

haematite plates has been mounted in a plastic box with non-magnetic glue in order to orient the samples in the sample holder. The low-field magnetic susceptibility measurements gave negative values of the k_3 axes. This is the result of the field dependency of magnetic susceptibility in large crystals of haematite as described in Hrouda (2002a). The orientation of the principal directions of AMS is correct, however, and not affected by field dependency.

4.1.1 Torque measurements

The high-field torque is characterized by asymmetry in the measurements perpendicular to the basal plane and a linear increase in amplitude with an increase in field strength (Fig. 3). Measurements within the basal plane ($x_2 - x_3$) show a small contribution of a 6θ term to the torque signal, which overlaps with the 2θ term (Fig. 3c). The 6θ term has been attributed to internal strain induced by twinning within the haematite basal plane (Flanders & Schuele 1964; Porath & Raleigh 1967). However, it is not possible to interpret the 6θ term precision as a result of its low intensity. The linear relationship between the torque amplitude and applied field confirms the validity of eq. (9) (Figs 3b, d and f).

The calculation of the coefficients of the torque resulting from the different magnetic components derived from eq. (2) illustrate that the paramagnetic (Figs 4a–c) and the ferrimagnetic fraction to the torque signal (Figs 4g–i) are statistically insignificant. The fact that we isolate a term that is dependent on either the square of the field or constant with the field suggests that torque is not perfectly linear to field. Error analysis, however, indicates whether these contributions actually have a statistical significance.

The haematite coefficient in a plane different than the crystal basal plane can be fit by the function described in eq. (9) with a solution that converges within a fiducial limit of 95 per cent confidence (Figs 4d and f). The solution of this best-fit function provides a mean orientation in the measured planes different from the basal plane. The obtained direction of the haematite *c*-axis is subparallel to the minimum-susceptibility axes measured by low-field methods (Fig. 5). The haematite coefficient in a plane subparallel to the crystal basal plane shows a 6θ coefficient that some authors have attributed to a trigonal susceptibility within the basal plane (Porath & Raleigh 1967) (Fig. 5e). At present, it is not possible to verify this is as a result of a trigonal component in these

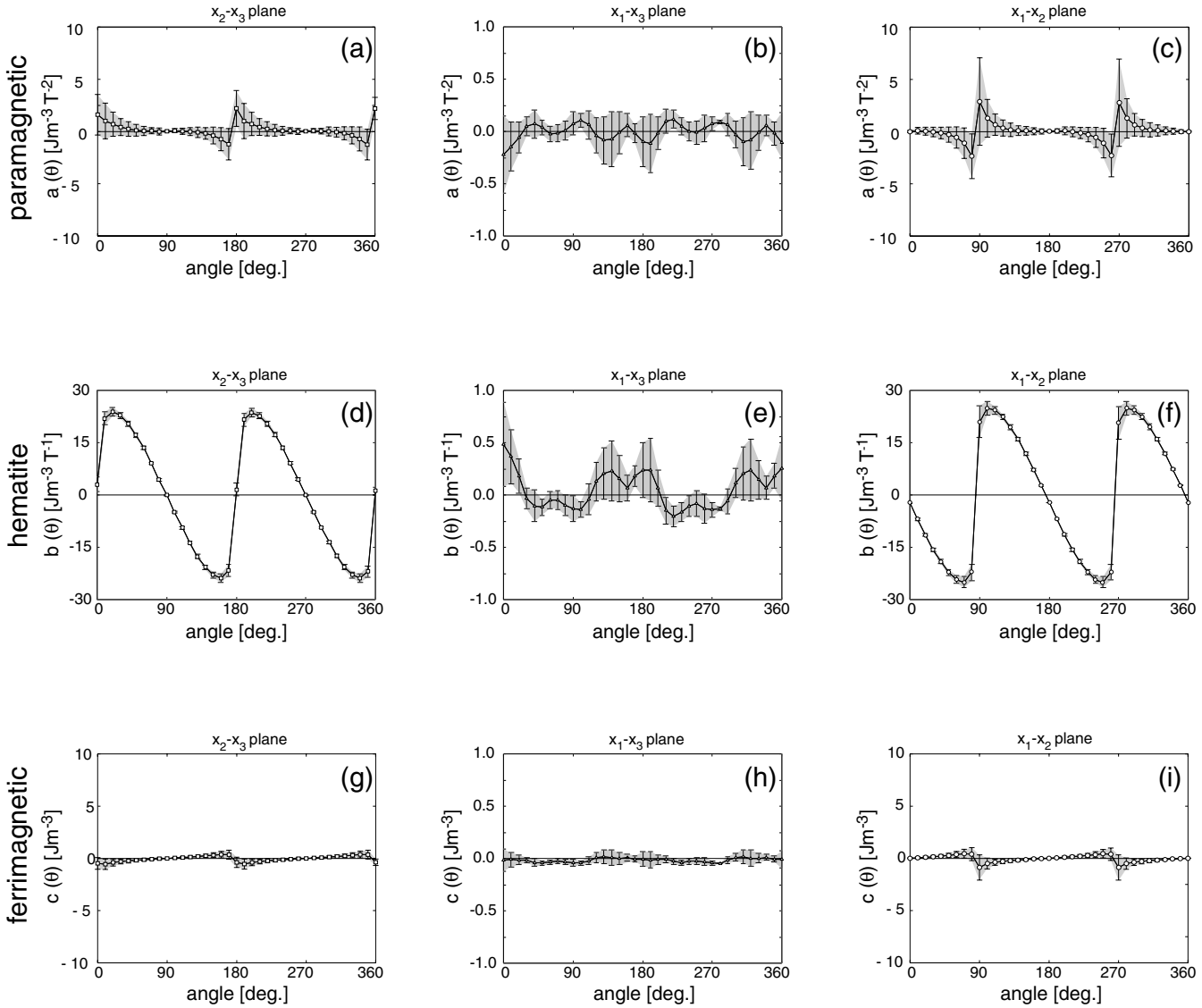

Figure 4. Separation of the torque signal of a haematite single crystal into the coefficients of the different magnetic components, where a(θ) corresponds to the paramagnetic coefficient in three perpendicular planes (a, b, c), b(θ) corresponds to the haematite coefficient (d, e, f) and c(θ) corresponds to the ferrimagnetic coefficient (g, h, i). The grey area indicates the 95 per cent confidence limit for each curve in this and subsequent figures.

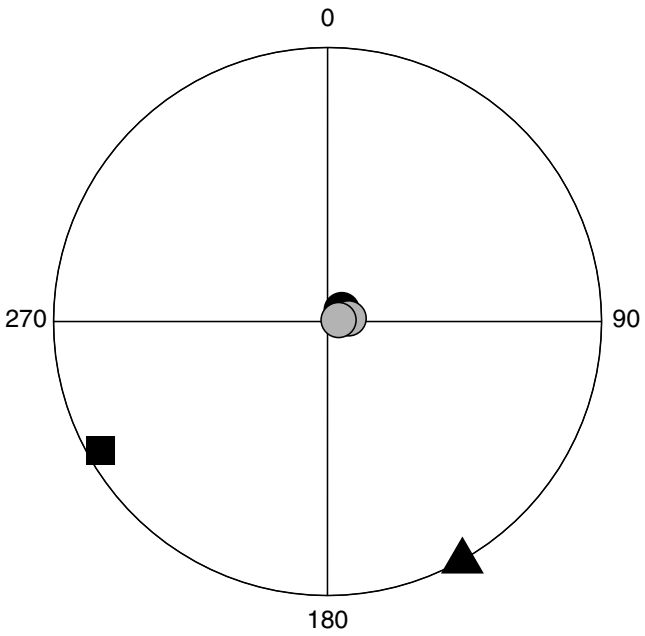

Figure 5. Direction of the principal axes of the AMS for a haematite single crystal. The low-field measurements are shown with black symbols and the haematite component of the high-field torque with grey. Squares, triangles and circles show the k_1, k_2 and k_3 axes, respectively, in this and subsequent figures.

crystals and more measurements would be required to confirm this hypothesis.

4.2 Deformed red beds

The palaeomagnetic direction and low-field AMS has been studied previously in the deformed Permian red beds from the Lower Glarus nappe complex (Hirt *et al.* 1986; Heller *et al*. 1989) . The finite strain has also been determined from reduction spots in the red shales/slates (Pfiffner & Ramsay 1982). The rocks have undergone extreme deformation, whereby the reduction spots are flattened in the cleavage plane and elongated in the direction of nappe transport (Pfiffner 1981). Hirt *et al.* (1986) found that the characteristic remanent magnetizations were distributed along a small circle away from the expected Permian direction. The amount of deflection, however, was not simply related to the degree of anisotropy. Ideally, it should be possible to use the magnetic fabric of haematite to correct the remanence deflection. Eight samples from the deformed red beds of the Lower Glaurus nappe complex in eastern Switzerland have been analysed to test the technique outlined above.

4.2.1 Magnetic mineralogy

The acquisition of IRM and subsequent thermal demagnetization of the IRM at maximum applied field is used in order to identify the magnetic minerals present in the samples (Lowrie 1990). The IRM acquisition curve shows the presence of a high-coercivity phase that does not saturate at the maximum applied field of 1 T (Fig. 6a). The concavity of the curve at low values of applied field does not show evidence of low-coercivity phases. The stepwise thermal demagnetization of the IRM acquired at 1.8 T indicates the presence of a high-coercivity component with a maximum unblocking temperature between 675° and 700° C (Fig. 6b). This magnetic mineral has been identified as haematite, as it has been suggested by Hirt *et al.* (1986).

4.2.2 Torque measurements

Eight samples we measured with the high-field torque magnetometer. The torque curves are characterized by an asymmetry, which is indicative of an antiferromangetic phase, in this case haematite (Figs 7a, c and e). A shifting of the torque signal with respect to the horizontal axes occurs as a result of the high rotational hysteresis of the haematite-bearing rocks (Owens 1981). The correlation between the amplitude of the torque signal and the applied field shows that paramagnetic phases also contribute to the torque signal: this is further corroborated by the fit of the second-order polynomial (Figs 7b, d and f).

The calculation of the coefficients of the torque resulting from the different magnetic components derived from eq. (2) reveals a statistically significant paramagnetic component (Figs 8a–c) and haematite component to the torque signal (Figs 8d–f). The ferrimagnetic component is not statistically significant, which would be expected from the rock magnetic experiments. More than 95 per cent of the data points are not different from zero within the estimated error (Figs 8g–i).

4.2.3 Magnetic anisotropy subfabrics

The results are analysed in terms of the orientation of principal directions of AMS, and the shape and degree of anisotropy of the susceptibility magnitude ellipsoid. The principal directions of the low-field AMS show good agreement with the paramagnetic susceptibility ellipsoid computed from high-field torque measurements

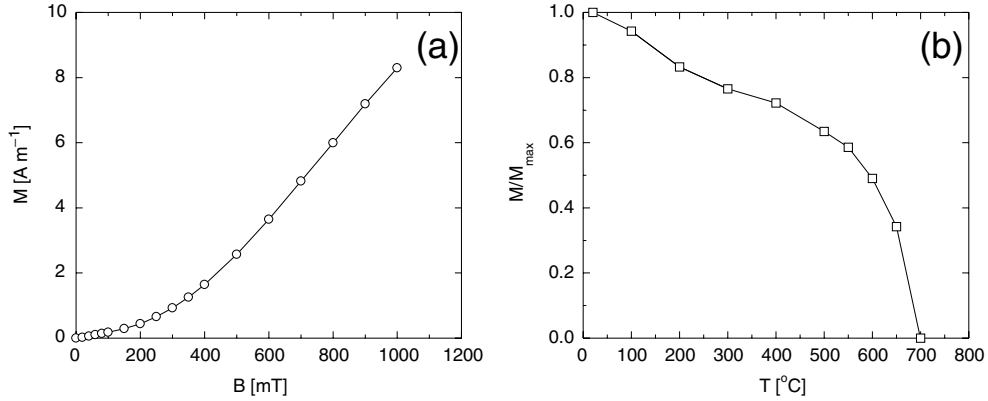

Figure 6. (a) IRM acquisition curve with remanent as a function of applied field for a representative specimen of red beds. (b) Thermal demagnetization of the single component.

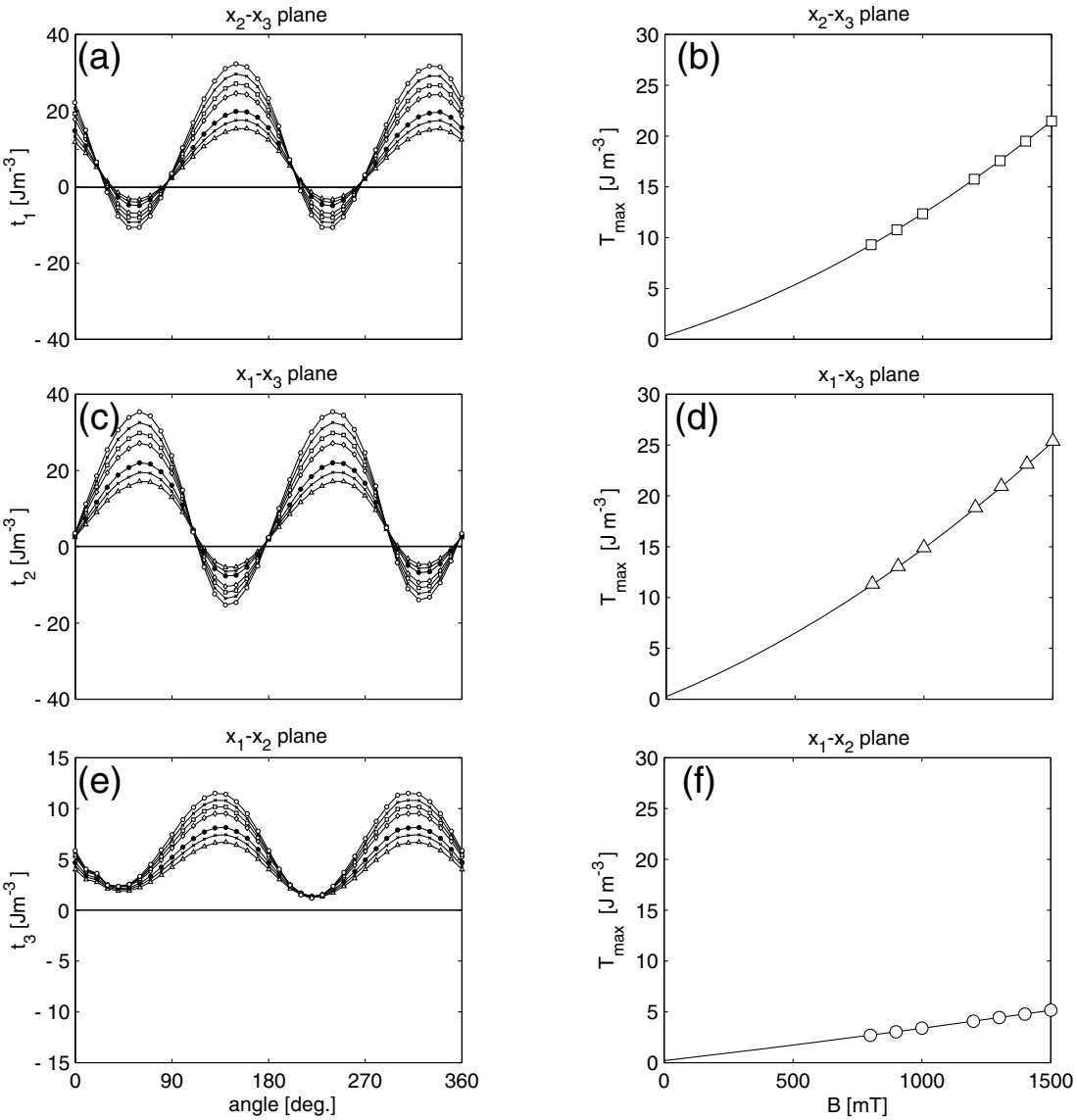

Figure 7. Torque curves (left) and corresponding amplitude of the torque signal (right) for a red-bed sample (GV10.01b). Plane $x_2 - x_3$ (a, b) and plane $x_1 - x_3$ (c, d) are perpendicular to cleavage and plane $x_1 - x_2$ parallel to cleavage (e, f) in this and Fig. 8.

(Fig. 9). The magnetic lineation, however, obtained by low-field measurements, is slightly better grouped than the paramagnetic lineation (Figs 9a and b). In order to investigate whether the paramagnetic susceptibility shows a well-defined magnetic lineation, the low-field magnetic susceptibility has been measured at 77 K, which enhances the paramagnetic susceptibility signal (Lüneburg *et al.* 1999; Parés & van der Pluijm 2002a). The orientation of the k_1 axes of the low-temperature AMS show a higher scattered distribution. This suggests that a ferromagnetic component also contributes to the low-field susceptibility and disperses the maximum susceptibility direction (Fig. 9a). The ratio between the bulk susceptibility measured at liquid nitrogen temperature and at room temperature was 3.8 with a correlation coefficient of 0.9998. This result justifies the assumption that a diamagnetic contribution to the anisotropy is insignificant and any quartz in the red beds does not contribute to the susceptibility.

A mean direction of the haematite *c*-axis is computed for each measurement plane, therefore, giving three mean directions per sample. For three planes in three different samples, the coefficient curve of the haematite did not converge to a non-linear fit of its theoretical function. The three poles to basal plane of haematite are then fitted by a small circle that gives the mean haematite *c*-axis direction for every sample. The obtained orientation of poles to haematite basal plane is the haematite minimum-susceptibility direction (Pfiffner & Ramsay 1982; Hrouda *et al.* 1985). The direction of minimum axes of susceptibility derived for haematite cluster around the pole to cleavage, however, also shows some deviation along a great circle perpendicular to the stretching lineation. If the haematite plates show some girdling within the cleavage plane, this configuration could lead to an apparent lineation, arising from haematite. A girdle orientation of the haematite *c*-axis has already been reported as the origin of magnetic lineation in haematite-bearing rocks by Rosiere *et al.* (1998) and Siemes *et al.* (2000).

Fig. 10 shows the shape of the paramagnetic and AMS ellipsoid as a function of the differences between k_1 and k_3 axes for the analysed red-bed samples. The shape of the ellipsoids are highly oblate for both the paramagnetic component of the high-field AMS and the low-field susceptibility, however, the shapes are slightly

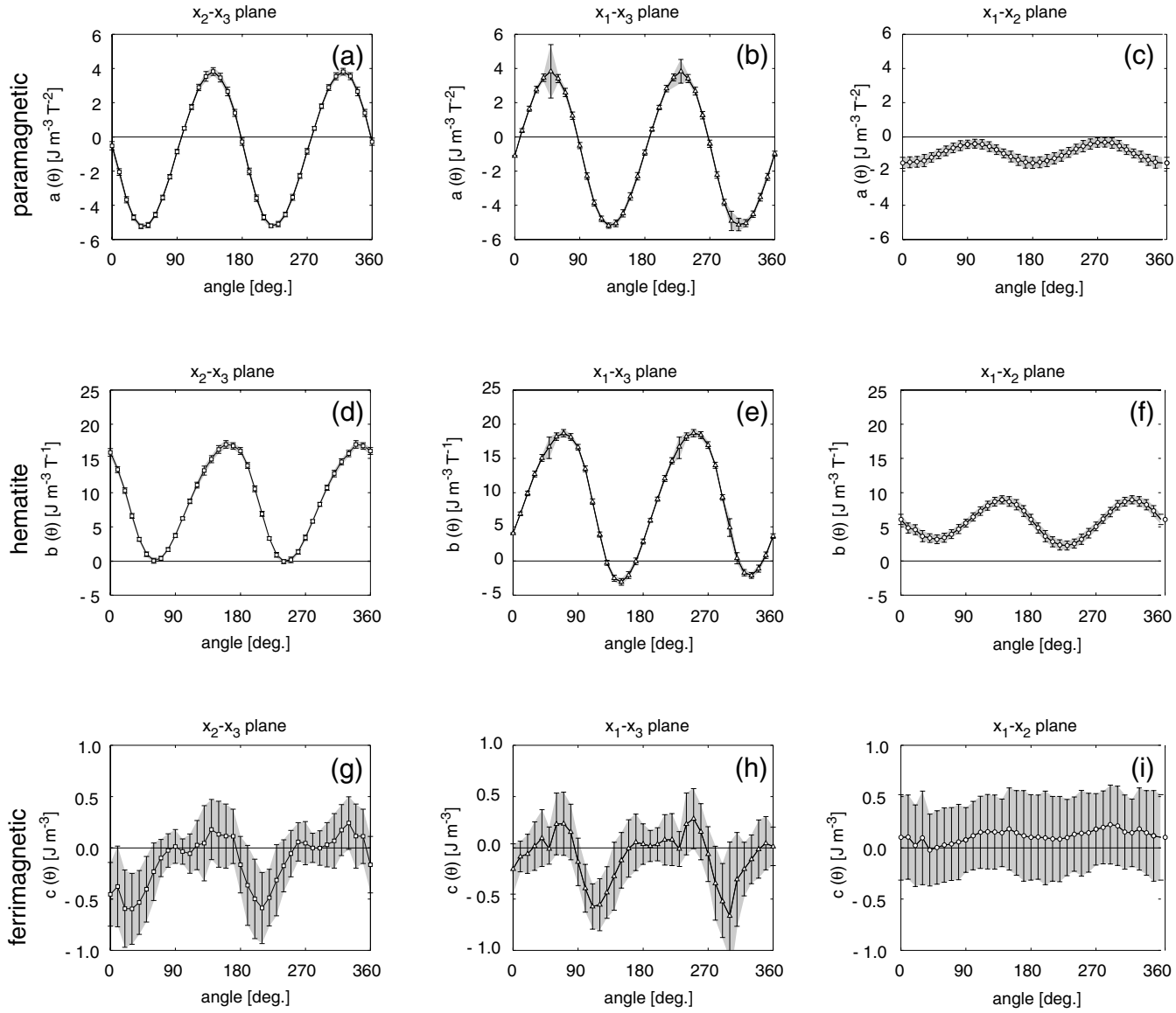

Figure 8. Separation of the torque signal of a red-bed sample (GV10.01b) into the coefficients of the different magnetic components, where a(θ) corresponds to the paramagnetic coefficient in three perpendicular planes (a, b, c), b(θ) corresponds to the haematite coefficient (d, e, f) and c(θ) corresponds to the ferrimagnetic coefficient (g, h, i).

better constrained for the paramagnetic tensor. The difference $k_1 - k_3$ in the low-field AMS ellipsoid is also more scattered. These differences are probably the result of the haematite contribution to the low-field anisotropy.

5 DISCUSSION

The method to separate a haematite component in high-field torque measurements is based on two assumptions: (i) the linear dependency of the torque resulting from haematite particles with respect to the applied field and (ii) the presence of an isotropic basal plane. The torque resulting from haematite is expressed in eq. (9) and includes a second term that accounts for the differences in the triaxial ellipsoid arising from the haematite magnetic susceptibility. Assuming measurements perpendicular to the basal plane, the torque can be expressed by $m_o H \sin\theta + \frac{1}{2}(\chi_\perp - \chi_{||})H^2 \sin 2\theta$, where $(\chi_\perp - \chi_{||})$ is the difference of the triaxial susceptibility of haematite perpendicular and parallel to the basal plane respectively. Using mean values derived from high-field torque on haematite crystals by Tasaki & Iida (1963) of $m_o = 0.36$ (A m^2 Kg^{-1}) and $\chi_\perp - \chi_{||}) = 9.8 \times 10^{-2}$ (A m^{-2} Kg^{-1} T^{-1}) it is found that the model of torque linear with applied field can be used in applied fields up to $B = 7$ T. It should be noted that the calculation is based on haematite single crystals. In aggregates and natural samples the limit is probably lower, however, it is valid in the range of fields used in this work.

The second assumption made in this study is the isotropic behaviour of the haematite basal plane. The 6θ term found in haematite single crystal curves within the basal plane could indicate a trigonal anisotropy in this plane, which has been interpreted as stress-induced anisotropy (Porath 1968) or magnetocrystalline anisotropy (Dunlop 1971). A strong uniaxial anisotropy has been observed within the haematite basal plane (Dunlop 1971). The theoretical model, which includes anisotropy within the basal plane, was proposed by Owens (1981). However, the good agreement between the haematite curves measured and the fitted function suggests that it is not necessary to include this effect in the separation method.

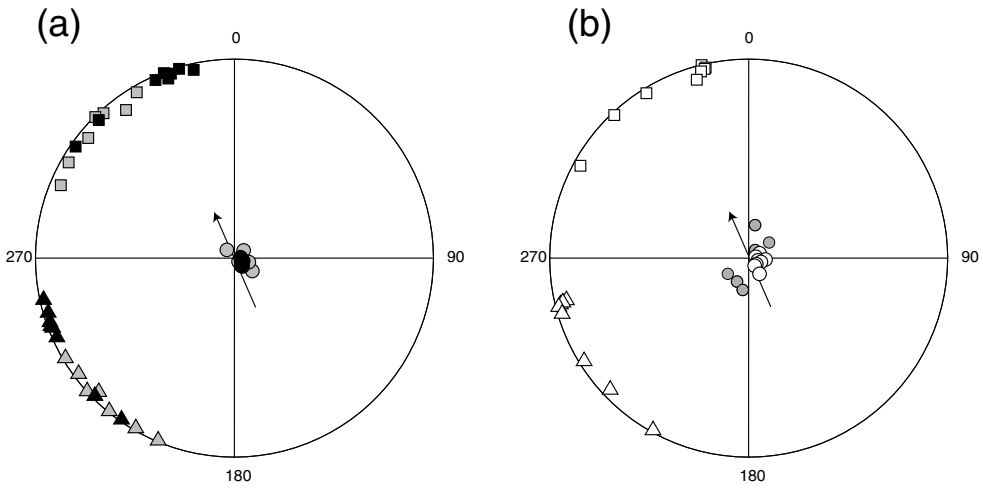

Figure 9. Orientation of the principal axes of magnetic anisotropy of eight samples in cleavage coordinates in red beds from the Lower Glarus nappe complex. (a) Principal axes of the low-field AMS measured at 293 K (black symbols) and low-field AMS at 77 K (grey symbols). (b) Paramagnetic susceptibility from high-field measurements (open symbols) and orientation of the haematite *c*-axis (grey circles). The arrow shows the direction of stretching lineation derived from reduction spots in the samples.

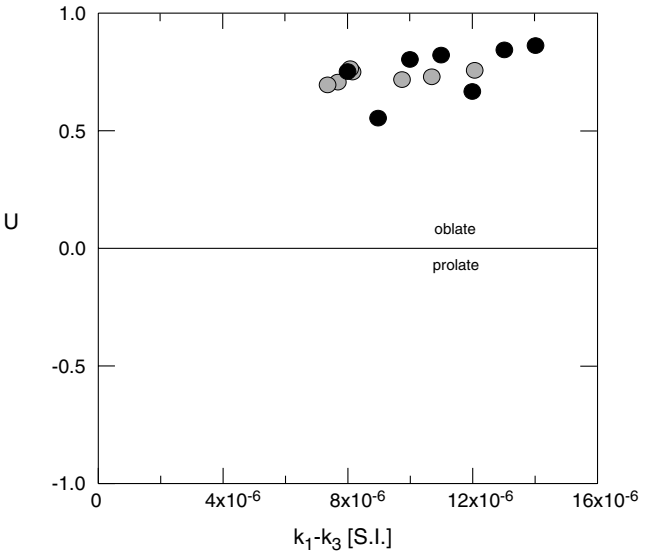

Figure 10. Shape parameter (U) as a function of the magnetic susceptibility differences for low-field AMS (black symbols) and the paramagnetic susceptibility (grey symbols).

The ferromagnetic moment calculated for the haematite fraction can be used as a proxy for the estimation of the haematite content in samples with different magnetic phases. The percentage of haematite will be the ferromagnetic moment, calculated from the fit, divided by the ferromagnetic moment of haematite single crystals. However, caution must be applied because the ferromagnetic moment of haematite single crystals has a wide variability and further analysis is necessary before a quantitative model can be established.

The linear relationship between applied field and torque is not only applicable to haematite but can also be found in pyrrhotite (Hirone *et al.* 1962; Bin & Pauthenet 1963; Sato *et al.* 1964; Friedrich *et al.* 1995). Potentially, the model could also be applied to pyrrhotite-bearing rocks, although, a reliable model that simulates the torque curve of pyrrhotite single crystals is required. However, the presence of differences in the iron content within the crystal and a possible trigonal anisotropy within the basal plane make the theoretical evaluation more difficult.

6 CONCLUSIONS

A new method for the separation of magnetic anisotropy components in haematite-bearing rocks has been developed: it allows for the separation of the magnetic anisotropy into the paramagnetic, ferromagnetic and haematite component. It has a main advantage over previous methods proposed by Rochette & Fillion (1988) and Bergmüller & Heller (1996) because with their approaches they could only identify the presence of haematite and calculate the magnetic anisotropy when haematite is the sole carrier of the AMS. The method presented here, not only, determines if haematite contributes to the AMS, it also calculates AMS ellipsoids for the paramagnetic and ferrimagnetic component and a mean direction of the haematite minimum-susceptibility direction.

By using a high number of applied fields, the measurements allow for the calculation of an error parameter for each of the magnetic anisotropy coefficients. This error parameter is used to discriminate the statistical significance of the components and their contribution to the torque signal. It is not possible, however, to calculate the full triaxial ellipsoid of magnetic susceptibility resulting from haematite; only the average orientation of poles to basal planes. Therefore, we recommend that several samples from the same site are analysed in order to evaluate possible girdle distributions of the haematite minimum-susceptibility direction.

ACKNOWLEDGMENTS

Funding for this project was provided by the Swiss National Science Funds with a postdoctoral fellowship. The authors would like to thank Roger Lacher for haematite single crystal measurements and Ramon Egli for his help with the long red-bed measurements. Ken Kodama and Mark Dekkers are gratefully acknowledged for their comments on an early version of the manuscript and J. M. Parés and F. Hrouda for their accurate revision.

REFERENCES

Banerjee, S.K. & Stacey, F.D., 1967. The high-field torque-meter method of measuring magnetic anisotropy in rocks, in *Methods in Palaeomagnetism,* pp. 470–476, ed. Runcorn, S.K., Elsevier, Amsterdam.

Bergmüller, F. & Heller, F., 1996. The field dependence of magnetic anisotropy parameters derived from high-field torque measurements, *Phys. Earth planet. Int.,* **96,** 61–76.

Bergmüller, F., Bärlocher, C., Geyer, B., Grieder, M., Heller, F. & Zweifel, P., 1994. A torque magnetometer for measurements of the high-field anisotropy of rocks and crystals, *Meas. Sci. Technol.,* **5,** 1466–1470.

Bin, M. & Pauthenet, 1963. Magnetic anisotropy of pyrrhotite, *J. Appl. Phys.,* **34,** 1161–1163.

Borradaile, G., Mothersill, J., Tarling, D. & Alford, C., 1985. Sources of magnetic susceptibility in a slate, *Earth planet. Sci. Lett.,* **76,** 336–340.

Borradaile, G.J. & Henry, B., 1997. Tectonic applications of magnetic susceptibility and its anisotropy, *Earth-Sci. Rev.,* **42,** 49–93.

Borradaile, G.J. & Werner, T., 1994. Magnetic anisotropy of some phyllosilicates, *Tectonophysics,* **235,** 223–248.

Brooks, P.J. & O'Reilly, W., 1970. Magnetic rotational hystresis characteristics of red sandstones, *Earth planet. Sci. Lett.,* **9,** 71–76.

Cheeney, R.F., 1983. *Statistical methods in geology,* George Allen & Unwin, London, p. 169.

Collinson, D.W., Creer, K.M. & Runcorn, S.K., 1967. *Methods in Palaeomagnetism,* Elsevier, Amsterdam, New York, p. 609.

Day, R., O'Reilly, W. & Banerjee, S.K., 1970. Rotational hysteresis study of oxidized basalts, *J. geophys. Res.,* **75,** 375–386.

Dunlop, D.J., 1971. Magnetic properties of fine-particle hematite, *Ann. Geophys.,* **27,** 269–293.

Dunlop, D.J. & Özdemir, Ö., 1997. *Rock Magnetism,* Cambridge Univ. Press, Cambridge, p. 573.

Flanders, P.J. & Remeika, J.P., 1965. Magnetic properties of hematite single crystals, *Philosophical Magazine,* **11,** 1271–1288.

Flanders, P.J. & Schuele, W.J., 1964. Anisotropy in the basal plane of hematite single crystals, *Philosophical Magazine,* **8,** 485–490.

Friedrich, D., Hrouda, F. & Chlapacova, M., 1985. Relationship between paramagnetic and ferrimagnetic anisotropies in selected specimens of the KTB borehole and its vicinity (German part of the Bohemian massif). *Sci. Drilling,* **5,** 3–15.

Heller, F., Lowrie, W. & Hirt, A.M., 1989. A review of palaeomagnetic and magnetic anisotropy results from the Alps, in: *Alpine Tectonics,* pp 399–420, eds Coward, H.P., Dietrich, D. & Park, R.G. The Geological Society Special Publications, 45, London.

Hirome, T., Adachi, K., Yamada, M., Chiba, S. & Tazawa, S., 1962. The magnetic anisotropy of pyrrhotite and iron selenide, *J. Phys. Soc. Jpn,* **17,** 257–260.

Hirt, A., Lowrie, W. & Pfiffner, O.A., 1986. A paleomagnetic study of tectonically deformed red beds of the Glarus nappe complex, eastern Switzerland, *Tectonics,* **5,** 723–731.

Hirt, A.M., Julivert, M. & Soldevila, J., 2000. Magnetic fabric and deformation in the Navia-Alto Sil slate belt, Northwestern Spain. *Tectonophysics,* **320,** 1–16.

Hounslow, M.W., 1985. Magnetic fabric arising from paramagnetic phyllosilicate minerals in mudrocks, *J. geol. Soc. Lond.,* **142,** 995–1006.

Hrouda, F., 1982. Magnetic anisotropy of rocks and its application in geology and geophysics, *Geophys. Surv.,* **5,** 37–82.

Hrouda, F., 2002a. Low-field variation of magnetic susceptibility and its effect on the anisotropy of magnetic susceptibility of rocks, *Geophys. J. Int.,* **150,** 715–723.

Hrouda, F., 2002b. The use of the anisotropy of magnetic remanence in the resolution of the anisotropy of magnetic susceptibility into its ferromagnetic and paramagnetic components, *Tectonophysics,* **347,** 269–281.

Hrouda, F. & Jelinek, V., 1990. Resolution of ferrimagnetic and paramagnetic anisotropies in rocks, using combined low-field and high-field measurements, *Geophys. J. Int.,* **103,** 75–84.

Hrouda, F., Siemes, H., Herres, N. & Hennig-Michaeli, C., 1985. The relationship between the magnetic anisotropy and the c-axis fabric in a massive hematite ore, *J. Geophys.,* **56,** 174–182.

Jackson, M., 1991. Anisotropy of magnetic remanence: a brief review of mineralogical sources, physical origins, and geological applications, and comparison with susceptibility anisotropy, *Pageoph,* **136,** 1–28.

Jelinek, V., 1978. Statistical processing of magnetic susceptibility measured on groups of specimens, *Stud. Geophys. Geod.,* **22,** 50–62.

Jelinek, V., 1981. Characterization of the magnetic fabric of rocks., *Tectonophysics,* **79,** T63–T67.

Jelinek, V., 1985. The physical principles of measuring magnetic anisotropy with the torque magnetometer, *Travaux de L'institut Geophysique de l'academie Tchecoslovaque des sciences,* **608,** 177–198.

Kelso, P.R., Tikoff, B., Jackson, M. & Sun, W., 2002. A new method for the separation of paramagnetic and ferromagentic susceptibility anisotropy using low field and high field methods, *Geophys. J. Int.,* **151,** 345–359.

Lowrie, W., 1990. Identification of ferromagnetic minerals in a rock by coercivity and unblocking temperature properties, *Geophys. Res. Lett.,* **17,** 159–162.

Lüneburg, C.M., Lampert, S.A., Lebit, H.K., Hirt, A.M., Casey, M. & Lowrie, W., 1999. Magnetic anisotropy, rock fabrics and finite strain in deformed sediments of SW Sardinia (Italy), *Tectonophysics,* **307,** 51–74.

Martín-Hernández, F. & Hirt, A.M., 2001. Separation of ferrimagnetic and paramagnetic anisotropies using a high-field torsion magnetometer, *Tectonophysics,* **337,** 209–221.

Martín-Hernández, F. & Hirt, A.M., 2003. Paramagnetic anisotropy of magnetic susceptibility biotite, muscovite and chlorite single crystals, *Tectonophysics,* **367,** 13–28.

McCabe, C., Jackson, M. & Ellwood, B.B., 1985. Magnetic anisotropy in the Trenton limestone: results of a new technique, anisotropy of anhysteretic susceptibility, *Geophys. Res. Lett.,* **12,** 333–336.

Owens, W.H., 1981. A simple model for non-vanishing rotational hysteresis in haematite, *Phys. Earth planet. Int.,* **27,** 106–113.

Parés, J.M. & van der Pluijm, B.A., 2002a. Phyllosilicate fabric characterization by Low-Temperature Anisotropy of Magnetic Susceptibility (LT-AMS), *Geophys. Res. Lett.,* **29**, article no. 2215.

Parés, J.M. & van der Pluijm, B.A., 2002b. Evaluating magnetic lineations (AMS) in deformed rocks, *Tectonophysics,* **350,** 283–298.

Pfiffner, O.A., 1981. Fold and thrust tectonics in the Helvetic Nappes (E. Switzerland), in *Thrust and Nappe Tectonics,* pp. 319–327, ed. Price. N.J., Geol. Soc. Lond., London.

Pfiffner, O.A. & Ramsay, J.G., 1982. Constraints on geological strain rates: Arguments from finite strain states of naturally deformed rocks, *J. geophys. Res.,* **87,** 311–321.

Porath, H., 1968. Stress induced magnetic anisotropy in natural single crystals of hematite, *Philosophical Magazine,* **17,** 603.

Porath, H. & Chamalaun, F.H., 1966. The magnetic anisotropy of hematite bearing rocks, *Pure appl. Geophys.,* **67,** 81–88.

Porath, H. & Raleigh, C.B., 1967. An origin of the triaxial basal-plane anisotropy in hematite crystals, *J. appl. Phys.,* **38,** 2401–2402.

Richter, C. & van der Pluijm, B.A., 1994. Separation of paramagnetic and ferrimagnetic susceptibilities using low temperature magnetic susceptibilities and comparison with high field methods, *Phys. Earth planet. Int.,* **82,** 111–121.

Rochette, P. & Fillion, G., 1988. Identification of multicomponent anisotropies in rocks using various field and temperature values in a cryogenic magnetometer, *Phys. Earth planet. Int.,* **51,** 379–386.

Rochette, P., Jackson, M. & Aubourg, C., 1992. Rock magnetism and the interpretation of anisotropy of magnetic susceptibility, *Rev. Geophys.,* **30,** 209–226.

Rosiere, C.A., Quade, H., Siemes, H. & Chemale, F., 1998. Fabric, texture and anisotropy of magnetic susceptibility in high-grade iron ores from the Quadrilatero Ferrifero, Minas Gerais, Brazil, in ed. Schwarzer, R.A., *Texture and Anisotropy of Polycrystals,* pp. 693–700, eds, Materials Science Forum. Zurich, Switzerland.

Sato, K., Yamada, M. & Hirome, T., 1964. Magnetocrystalline anisotropy of pyrrhotite, *J. Phys. Soc. Jpn,* **19,** 1592–1595.

Schmidbauer, E. & Keller, R., 1996. Magnetic properties and rotational hysteresis of Fe_3O_4 and γ-Fe_2O_3 particles 250 nm in diameter, *Journal of Magnetism and Magnetic Materials,* **152,** 99–108.

Siemes, H., Schaeben, H., Rosiere, C.A. & Quade, H., 2000. Crystallographic and magnetic preferred orientation of hematite in banded iron ores, *J. Struct. Geol.,* **22,** 1747–1759.

Tarling, D.H. & Hrouda, F., 1993. *The Magnetic Anisotropy of Rocks,* Chapman & Hall, London, p. 217.

Tasaki, A. & Iida, S., 1963. Magnetic properties of synthetic single crystal of α-Fe_2O_3, *Journal of the Physical Society of Japan,* **18,** 1148–1154.

Townsend, T., 1920. Magnetization and hysteresis in hematite crystals., *Phys. Rev.,* **15,** 345–364.